Fall 12-2021

Iron Geochemistry Across an Estuary-to-Coastal Gradient

Lissett G. Diaz
lgdiaz@coastal.edu

Iron Geochemistry Across an Estuary-to-Coastal Gradient

By

Lissett G. Diaz

Marine Science

Submitted in Partial Fulfillment of the
Requirements for the Degree of Bachelor of Science
In the HTC Honors College at
Coastal Carolina University

Fall 2021

Louis E. Keiner
Director of Honors
HTC Honors College

Angelos K. Hannides
Associate Professor
Department of Marine Science
Gupta College of Science

Table of contents

Abstract

Iron is a ubiquitous earth element that participates in biogeochemical processes that occur in marine sediments. Microorganisms utilize iron for many purposes, including cell growth, conserving energy, and for maintaining metabolic activity. In coastal sedimentary settings, understanding the redox reactions involving ferric iron, Fe^{3+}, and ferrous iron, Fe^{2+}, in its solid phase and pore-water phases, respectively, enable an appreciation of biogeochemical transformations occurring in the coastal zone. In this study, iron concentrations in sediment of ranging permeability were determined at four stations marking an estuary-coast transition zone in Singleton Swash in Myrtle Beach, South Carolina. The findings of the study indicate that the stations of highly permeable sediments and large grain sizes are characterized by greater concentrations of $[Fe^{2+}]$ and $[Fe]_D$, and are likely dominated by suboxic processes.

Introduction

Iron is one of the most abundant elements on Earth playing a critical role in geochemical cycling. Marine sediments are the site of many biogeochemical processes and supply iron to overlying surface waters (Burdige and Komada, 2020). More specifically, the interactions between metabolic activity of organisms, e.g., cell growth and conservation of energy, and redox-reactions that occur in marine sediments are vital in understanding the role of iron and the enzymatic processes affecting the distribution of iron. (Burdige and Komada, 2020; Shulz and Zabel, 2006). Iron can become more bioaccessible to organisms after reduction from Fe^{3+}, which is found in the solid phase, to Fe^{2+}, which is found in the dissolved phase. The produced dissolved iron in sediments diffuses upwards (or is transported upwards in the case of permeable sediments) resulting in reactive iron oxides after exposure to oxygen. This produces an enriched iron oxide layer of the sediment column (Burdige et al., 2020; Scholz et al., 2016).

Pore water studies are fundamental in investigating the oxidation of organic matter and the process of early diagenesis in the sediment and water column (Froelich et al., 1979). The processes of diagenesis are based on reactions that occur at varying depths depicted through concentration profiles (Shulz and Zabel, 2006). The distribution of the reactants and products of biogeochemical reactions will be affected in part by sedimentary properties, e.g. porosity, permeability, and grain size distribution, that will be affected in turn the rates of diffusion and advective transport (Anschutz and Charbonnier, 2021).

Porewater and solid-phase analysis have been previously done on eutrophic estuaries of sulfide- rich sediments to determine the role of sulfide in pyrite (FeS_2) formation. Sediment cores were obtained and were analyzed chemically using various methods such as 1,10 phenanthroline

method and molybdenum blue method to determine dissolved Fe^{2+} and dissolved total sulfide, respectively (Kraal et al., 2013). The 1,10-phenanthroline method (APHA, 2005) found that iron was predominantly found in its reactive form and showed extensive sulfidization (e.g., FeS and FeS_2) regardless of the oxygenated overlying water. Kraal et al. (2013) found that Fe sulfidization was driven by the reductive process in anoxic sediments and rapid burial of fine-grained sediments.

More recently, pore-water samples in sandy permeable sediments were extracted from sediment core slices to analyze various dissolved compounds (Fe^{2+}, Mn^{2+}, NH_4^+, etc.) in the sample (Anschutz and Charbonnier, 2021). The goal was to identify benthic biological processes by sampling sandy sediments with a vertical resolution of 1 cm by taking into account sedimentary properties. Fe oxides were detected in the first few centimeters and a rise in Fe^{2+} concentrations, less than 2 µM, was detected deeper than 15 cm depth. This observation including the concentrations of increased Mn^{2+} concentrations, indicated that early diagenesis was driven by these redox reactions (Anschutz and Charbonnier, 2021). Due to the relative lack of studies that describe the concentrations of dissolved and solid-phase compounds such as iron in sandy permeable sediments in comparison to muddy sediments, the distribution of total dissolved iron, $[Fe]_D$ and ferric iron, $[Fe^{2+}]$, from an estuary-to-coastal gradient is widely unknown.

This study aims to increase the understanding of iron reduction and total dissolved iron influenced by various sedimentary properties such as permeability, grain size, and porosity patterns in both muddy and sandy sediments and the role of biogeochemical processes. Porewater data collected from sediments in Singleton Swash in Myrtle Beach, South Carolina

will be used to illuminate the significance of iron geochemistry in the estuary-to-coastal gradient in these sedimentary properties.

Hypotheses

<u>Overarching Hypothesis:</u> Iron concentrations will be higher in mud versus sand due to lower permeability, smaller grain size, and slower exchange with overlying water.

Hypothesis 1: Muddy sediments will have higher concentrations of total iron due to smaller grain sizes and smaller pores permitting mainly molecular diffusion, as compared to coarser sand sediments with larger pores that permit advective transport.

Hypothesis 2: Low-permeable sediments will have higher concentrations of iron than sediments with higher permeability which would allow faster release of iron into the water column.

Hypothesis 3: The landward-most station will have higher concentrations of total iron, as opposed to the oceanward-most station at the creek outflow of the primary channel, due to greater buildup of iron.

Methods

Study Site

The study site was located in Singleton Swash, Myrtle Beach in South Carolina (Figure 1), an estuarine tidal creek emptying into Long Bay through a sandy beach. The 4 stations sampled during this study were located along a land-to-ocean transect along the creek.

Figure 1. Study site and stations in Singleton Swash, South Carolina obtained from overlayed image on Google Earth from 02/04/2020. Station 1 was located at tidal creek outflow sampled on 10/22/2021.

Field Observations

Prior to sampling, the parameters latitude, longitude, dissolved O_2, salinity, and temperature were measured using a YSI ProDSS meter with a temperature-conductivity-oxygen sensor and a built-in GPS. Additionally, the distance between stations was measured through Google Earth using the exact location from oceanward most station to the landward-most station.

Table 1: The water characteristics (distance from most oceanward station to most landward location, salinity, temperature) along the estuarine creek measured during sampling recorded on 10/22/2021. The distance was measured along the primary channel from the oceanward-most station 1 at 0 m.

Property	**Station 1**	**Station 2**	**Station 3**	**Station 4**
Distance (m)	0	268	390	562
Latitude	33.75623	33.75633	33.75742	33.75846
Longitude	-78.792	-78.79465	-78.79435	-78.79301
Dissolved O_2 (mg L^{-1}, mean ± 1 s.d.)	6.8 ± 0.006	50.1 ± 0	51.1 ± 0	49.8 ± 0.02
Salinity (PSU, mean ± 1 s.d.)	33.1 ± 0.03	33.3 ± 0	33.1 ± 0	33.8 ± 0.006
Temperature (°C, mean ± 1 s.d.)	25.0 ± 0.05	24.3 ± 0	25.5 ± 0	24.7 ± 0
Sulfidic Smell	None	None	Mild	Intense

Sampling

Duplicate surface water samples and pore-water samples were retrieved using a pure titanium MHE PushPoint sampler (MHE Products, East Tawas, MI, USA) from 15-cm increments beneath the sediment surface. Samples were retrieved using a 50-mL polypropylene-polyethylene syringe, then transferred by tubing into a 5-mL syringe and were filtered on site through a 0.2µm nylon-membrane in-line filters. The filtered samples were dispensed using a 1-mL syringe into microcentrifuge tubes containing Ferrozine reagent and hydroxylamine solution for Fe(II) and total dissolved Fe analysis, respectively (see below). Additionally, sediment samples from the top 5-10 cm were collected directly into pre-weighed vials and plastic containers for permeability, grain size and porosity analysis.

Laboratory Analysis

Permeability was determined using the constant-head method (Klute et al., 1989; Rocha et al., 2005). Grain size distribution was determined by wet sieving (McManus, 1988). Porosity was measured thermogravimetrically (Breitzke 2006). Samples were analyzed for Fe(II) ($[Fe^{2+}]$) and Total Dissolved Fe ($[Fe]_D$) by spectrophotometry using the Ferrozine method (Stookey, 1970).

Data Analysis

All graphing and statistical analysis were performed using MS Excel (Microsoft). Property-property plots of average permeability vs average concentrations, grain size vs. average concentrations, and distance vs average concentrations were created to address hypotheses 1, 2 and 3, respectively.

Results

Sedimentary Properties

Sedimentary and physical properties are summarized in Table 2. Overall, permeability decreases as grain size decreases, and porosity increases. Station 2 has the highest permeability ($>10^{-12}$ m^2). The percent contribution of fines (<63 μm) to total sediment mass increases as the permeability decreases. Additionally, Station 4 was classified as being poorly sorted in comparison to stations 1, 2, and 3 being moderately well sorted, moderately well sorted, and moderately sorted, respectively. More particularly, Station 2 exhibited a skewness that was positive while the rest of the stations were symmetrical.

Table 2. Sedimentary geological properties of the four stations sampled (mean ± standard deviation). The sorting and skewness statistics and qualitative classification were determined according to McManus (1988).

Property	Station 1	Station 2	Station 3	Station 4
Permeability (m^2)	$3.2x10^{-11} \pm 3.1x10^{-13}$	$4.4x10^{-11} \pm 3.6x10^{-12}$	$2.7x10^{-12} \pm 5.6x10^{-14}$	$5.9x10^{-13} \pm 1.3x10^{-14}$
Porosity	0.37 ± 0.003	0.38 ± 0.007	0.44 ± 0.02	0.49 ± 0.007
Mean grain size (phi)	1.70	1.93	2.14	2.64
Mean grain size (µm)	307	263	227	151
Median grain size (phi)	1.70	1.86	2.11	2.73
Median grain size (µm)	307	276	232	161
Percent Fines (<63 µm)	1.0	0.9	3.0	8.0
Sorting, σ_1	0.66	0.699	0.752	1.065
Sorting, classification	Moderately well sorted	Moderately well sorted	Moderately sorted	Poorly sorted
Skewness, SK_1	0.01	0.17	0.05	0.09
Skewness, classification	Symmetrical	Positively skewed	Symmetrical	Symmetrical

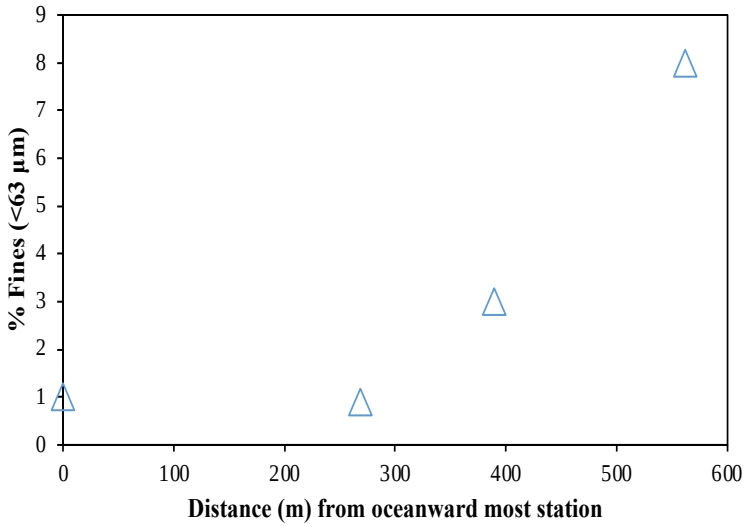

Figure 2. Percent fines along the transition of the estuarine tidal creek. Distance of 0 m indicates the creek outflow (Station 1; Figure 1).

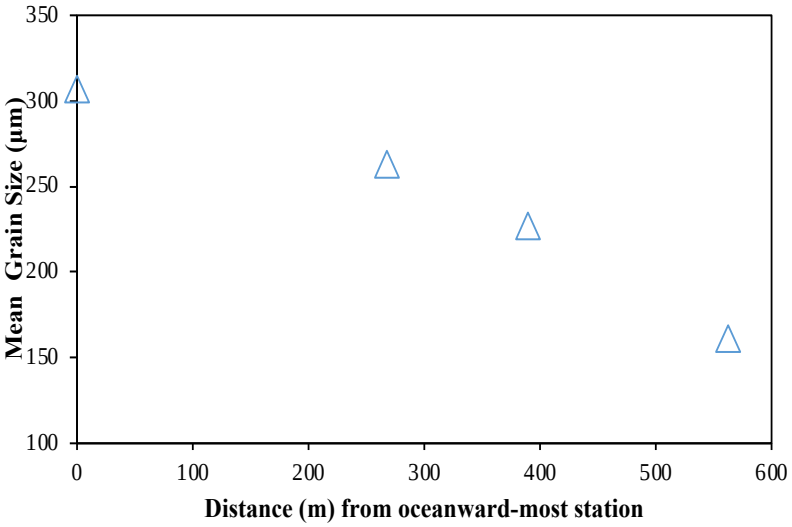

Figure 3. Mean grain size along the transition of the estuarine tidal creek. Distance of 0 m indicates the creek outflow (Station 1; Figure 1).

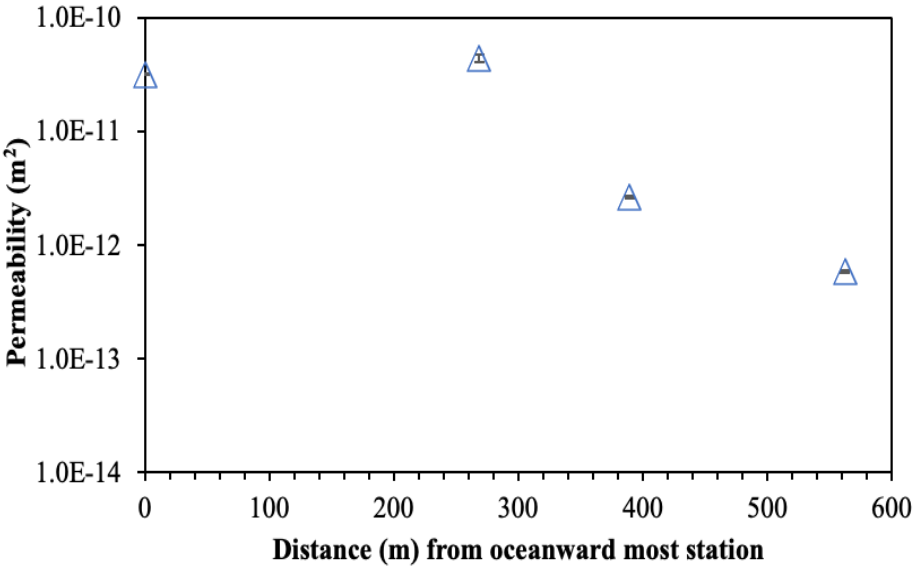

Figure 4. Sediment permeability along the estuarine tidal creek. Distance of 0 m indicates the creek outflow (Station 1; Figure 1).

Porewater Iron Concentrations

The average concentration of $[Fe^{2+}]$ μmol L^{-1} and $[Fe]_D$ μmol L^{-1} for each station are summarized in Table 3. Figure 5 shows pore-water profiles of $[Fe^{2+}]$ and $[Fe]_D$. $[Fe^{2+}]$ is highest at Station 2 at 60 cm and $[Fe]_D$ is largest at Station 1 at 90 cm. Station 4 only represented three depths due to inability to insert the titanium core further than 25 cm. Figure 6 shows $[Fe^{2+}]$ profiles in Station 1 and Station 3 in a concentration scale different than in Figure 5.

Table 3. Descriptive statistics of various properties for $[Fe^{2+}]$ μmol L^{-1} and $[Fe]_D$ μmol L^{-1} at each of the four stations at Singleton Swash in Myrtle Beach, South Carolina.

	$[Fe^{2+}]$ μmol L^{-1}				**$[Fe]_D$ μmol L^{-1}**			
Station	**1**	**2**	**3**	**4**	**1**	**2**	**3**	**4**
Average	1.134	6.855	1.263	0.182	20.685	6.670	1.676	0.595
St. Dev.	±1.505	±15.828	±0.998	±0.174	±27.316	±14.025	±0.983	±0.152
Count	12	12	12	6	12	12	12	6
Max.	4.09416	43.1688	2.550	0.465	79.233	38.923	3.092	0.775
***z* (cm)**	90	60	30	25	90	60	30	25
Min.	-0.0759	-0.0759	-0.0759	0.001	0.3116	0.312	0.312	0.466
***z* (cm)**	0	15, 30, 35	0	0	15	15, 45	0	0, 15

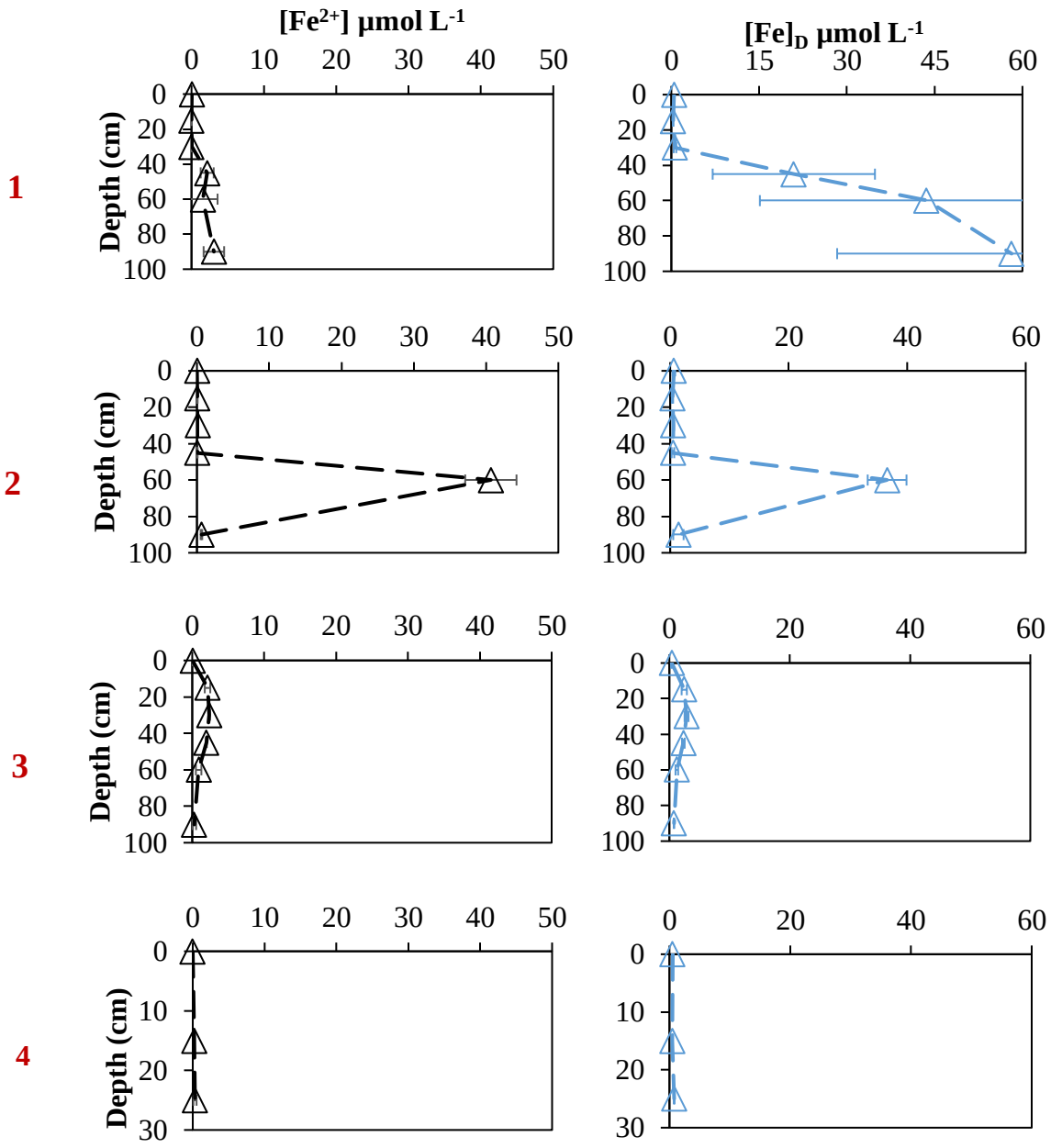

Figure 5. Eight depth-profiles developed from four stations containing two profiles of average $[Fe^{2+}]$ and $[Fe]_D$ µmol L^{-1} from duplicate sample profiles from the Estuarine Tidal Creek. In Station 4, a full profile was not developed due to the inability to insert the titanium core deeper through the sediment (Figure 2).

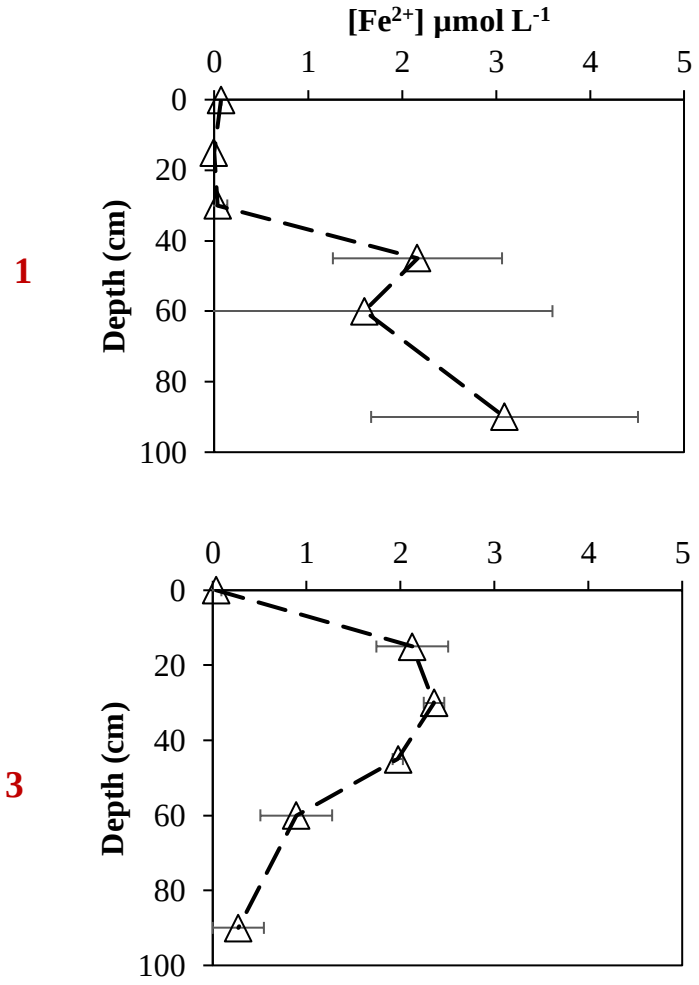

Figure 6. Sedimentary [Fe^{2+}] profiles at Stations 1 and 3.

Iron vs Mean Grain Size (Hypothesis 1)

Figure 7 shows as mean grain size increases, $[Fe^{2+}]$ and $[Fe]_D$ increases. The lowest concentrations of $[Fe^{2+}]$ and $[Fe]_D$ coincided with the lowest mean grain size at Station 4.

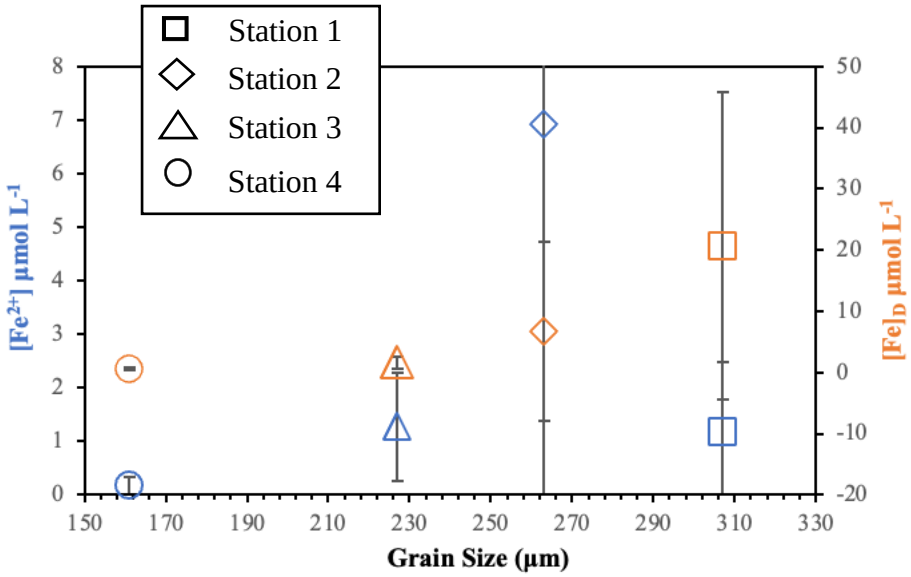

Figure 7. Average $[Fe^{2+}]$ µmol L^{-1} and $[Fe]_D$ µmol L^{-1} at each of the four stations against the mean grain size at each station.

Iron vs Permeability (Hypothesis 2)

Figure 8 shows as permeability (m^2) increases, $[Fe^{2+}]$ and $[Fe]_D$ increases. The lowest concentrations of $[Fe^{2+}]$ and $[Fe]_D$ coincided with the lowest permeability at Station 4.

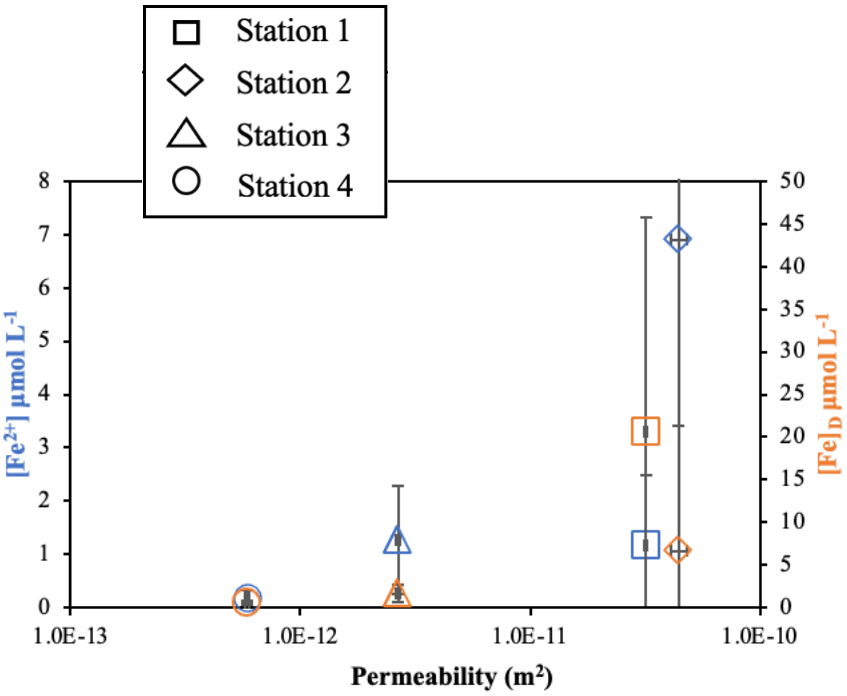

Figure 8. Average $[Fe^{2+}]$ µmol L^{-1} and $[Fe]_D$ µmol L^{-1} at each of the four stations against permeability.

Iron vs Distance (Hypothesis 3)

Figure 9 shows that $[Fe]_D$ is at its highest concentration at the creek outflow (Station 1) and decreases into the estuary. At station 4, $[Fe^{2+}]$ and $[Fe]_D$ were minimal.

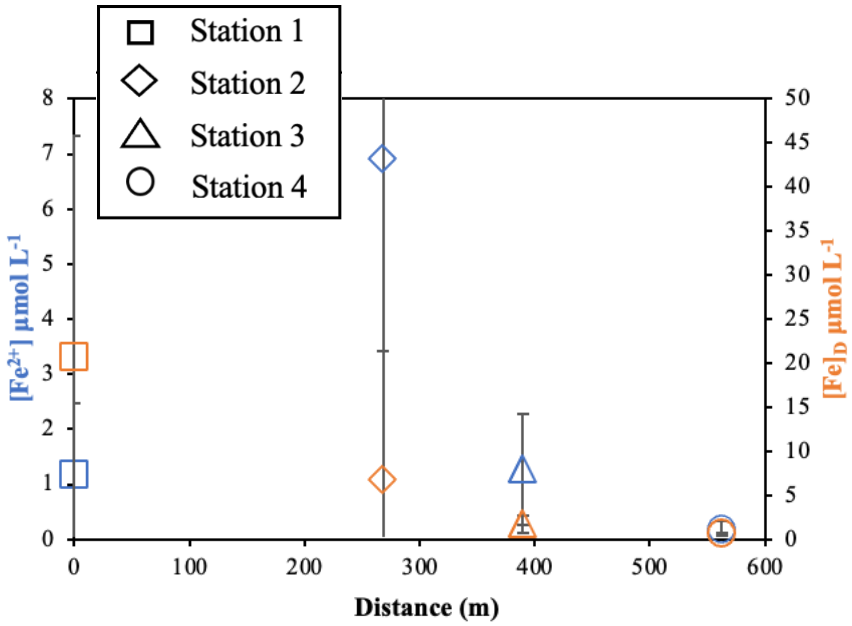

Figure 9. Average $[Fe^{2+}]$ µmol L^{-1} and $[Fe]_D$ µmol L^{-1} at each of the four stations against distance. Distance of 0 m indicates the creek outflow (Station 1; Figure 1).

Discussion

Sedimentary Geochemical Profiles

In Station 1(Figure 6), there is a distinct transition between depths of 0-30 cm, and of 45-90 cm. This significant difference can be a consequence of bioturbation involving animal burrows in sediments that affect the biogeochemical processes. Ghost shrimp (*Neotrypaea californiensis*) is a crustacean that inhabits sandy sediments and provide pressure for pore-water and results in movement of sediment along with highly permeable sediment essentially creating bioadvective transport (Volkenborn et al., 2012). This is supported by the wave and currents that dominate due to the high energy environment in more permeable sediments. A similar trend appeared for the $[Fe]_D$ μmol L^{-1} profile at Station 2.

In Station 2, the highest average concentration of $[Fe^{2+}]$ is at the depth of 60 cm (Table 3, Figure 5). As depth increases, suboxic zones begin to dominate. This results in Fe^{3+} reduction mediated by microorganisms resulting in Fe^{2+} via anerobic respiration. The same trend appeared for the $[Fe]_D$ μmol L^{-1} profile at Station 2.

In Station 3(Figure 6), the pore-water profile is representative of a subtropic column where iron reduction is occurring at 15-45 cm depth. The profiles developed for Station 3 for both $[Fe^{2+}]$ μmol L^{-1} and $[Fe]_D$ μmol L^{-1} are indicative of diffusion transport dominating this site which correlates with the low permeability of 2.7×10^{-12} $m^2 \pm 5.6\times10^{-14}$.

Station 4 exhibited concentrations of both $[Fe^{2+}]$ μmol L^{-1} and $[Fe]_D$ μmol L^{-1} below 1 μmol L^{-1}. This is most likely due to the domination of sulfide reduction as anoxic zones begin to dominate and the formation of FeS compounds.

Sedimentary Geochemical Patterns

The results strongly indicate that permeability and grain size have the strongest correlation to the concentrations of ferric iron and total dissolved iron. The contribution of fines (<63 μm) increases from the oceanward most station at the creek outflow to the landward most station towards the estuary, as mean grain size decreases. The highest average concentrations of $[Fe^{2+}]$ μmol L^{-1} and $[Fe]_D$ μmol L^{-1} at station 1 and station 2 were found in coarser sandy sediments of higher mean grain size. On the other hand, lower-concentrations of $[Fe^{2+}]$ μmol L^{-1} and $[Fe]_D$ μmol L^{-1} were found in finer sediments of lower mean grain size. Similarly, sedimentary permeability exhibited a similar trend to grain size. Sedimentary permeability is decreasing from the oceanward most station at the creek outflow to the landward most towards the estuary. Thus, as permeability increases, the average concentrations of $[Fe^{2+}]$ μmol L^{-1} and $[Fe]_D$ μmol L^{-1} increase. Therefore, both mean grain size and permeability experience a direct relationship with concentration.

The trends indicate that as permeability and grain size decrease, oxygen supply decreases as the depth increases further down the sediment column. The mild sulfidic smell and intense sulfidic smell in Station 3 and in Station 4, respectively, are prominent. Oxidized iron was observed (orange color) at the surface layer sediment obtained from Station 3 along with a distinct black color in the mud observed in both Station 3 and Station 4. This shows that at these two stations, sulfate reduction takes place. When sulfide is in the presence of iron, both iron

monosulfide (FeS) and as pyrite (FeS_2) precipitates (Krall et al., 2013). This results in a decrease of $[Fe^{2+}]$ μmol L^{-1} and $[Fe]_D$ μmol L^{-1} at stations with finer grains and low-permeable sediments.

Conclusion

The findings of the study indicate that the stations of highly permeable sediments and large grain sizes are characterized by greater concentrations of $[Fe^{2+}]$ and $[Fe]_D$. The most likely explanation for these trends lies with oxygen supply from overlying water: as permeability and grain size decrease, oxygen supply decreases and the sediment column becomes anoxic, sulfate reduction dominates and sulfide forms FeS compounds with dissolved iron. These results contribute to understanding iron geochemistry across an estuary-to-coastal gradient.

Acknowledgments

I would like to give a special thank you to my advisor, Dr. Angelos Hannides, for their mentorship and for giving me the opportunity to grow as a young scientist through my Honors Thesis experience. This project would not have been possible without his guidance and ability to obtain materials necessary for the method. This was also accomplished with the support from Coastal Carolina University's HTC Honors College.

Literature Cited

APHA (2005). American Public Health Association – American Water Works Association – Water Environment Federation. *Standard Methods for the Examination of Water and Wastewater*, 21ed.

Anschutz, P., & Charbonnier, C. (2021). Sampling pore water at a centimeter resolution in sandy permeable sediments of lakes, streams, and coastal zones. *Limnology and Oceanography: Methods*, *19*(2), 96–114. https://doi.org/10.1002/lom3.10408

Breitzke, M (2006) Physical properties of marine sediments, In *Marine Geochemistry*, Schulz, HD, and Zabel, M (Eds), Springer, 27-71.

Burdige, D. J., & Komada, T. (2020). Iron redox cycling, sediment resuspension and the role of sediments in low oxygen environments as sources of iron to the water column. *Marine Chemistry*, *223*, 103793. https://doi.org/10.1016/j.marchem.2020.103793

Froelich, P. N., Klinkhammer, G. P., Bender, M. L., Luedtke, N. A., Heath, G. R., Cullen, D., Dauphin, P., Hammond, D., Hartman, B., & Maynard, V. (1979). Early oxidation of organic matter in pelagic sediments of the eastern equatorial Atlantic: Suboxic diagenesis. *Geochimica et Cosmochimica Acta*, *43*(7), 1075–1090. https://doi.org/10.1016/0016-7037(79)90095-4

Klute, A.; Dirksen, C. Hydraulic Conductivity and Diffusivity: Laboratory Methods; Klute, A., Ed.; SSSA Book Series; American Society of Agronomy—Soil Science Society of America: Madison, WI, USA, 1986; pp. 687–734

Kraal, P., Burton, E. D., & Bush, R. T. (2013). Iron monosulfide accumulation and pyrite formation in eutrophic estuarine sediments. *Geochimica et Cosmochimica Acta*, *122*, 75–88. https://doi.org/10.1016/j.gca.2013.08.013

McManus, J. Grain Size Determination and Interpretation. In *Techniques, in Sedimentology*; Tucker, M., Ed.; Blackwell Scientific Publications: Oxford, UK, 1988; pp. 63–85.

Rocha,C.;Forster,S.;Koning,E.;Epping,E.High-resolutionpermeabilitydeterminationandtwo-dimensional porewater flow in sandy sediment: High-resolution permeability gradients in sands. Limnol. Oceanogr. Methods 2005, 3, 10–23.

Scholz, F., Löscher, C. R., Fiskal, A., Sommer, S., Hensen, C., Lomnitz, U., Wuttig, K., Göttlicher, J., Kossel, E., Steininger, R., & Canfield, D. E. (2016). Nitrate-dependent iron oxidation limits iron transport in anoxic ocean regions. *Earth and Planetary Science Letters*, *454*, 272–281. https://doi.org/10.1016/j.epsl.2016.09.025

Schulz, HD, and Zabel, M (2006) Marine Geochemistry, Springer.

Stookey, Lawrence L. 1970. "Ferrozine---a New Spectrophotometric Reagent for Iron." *Analytical Chemistry* 42 (7): 779–81.

Volkenborn, N., Polerecky, L., Wethey, D., Dewitt, T., & Woodin, S. (2012). *Hydraulic activities by ghost shrimp Neotrypaea californiensis induce oxic-anoxic oscillations in sediments*. https://doi.org/10.3354/MEPS09645